Structure and Dynamics of Supercooled Liquid $Ge_2Sb_2Te_5$ from Machine-Learning-Driven Simulations

Yu-Xing Zhou, Han-Yi Zhang, Volker L. Deringer,* and Wei Zhang*

Studies of supercooled liquid phase-change materials are important for the development of phase-change memory and neuromorphic computing devices. Herein, a machine-learning (ML)-based interatomic potential for $Ge_2Sb_2Te_5$ (GST) to conduct large-scale molecular dynamics simulations of liquid and supercooled liquid GST is used. A pronounced effect of the thermostat parameters on the simulation results is demonstrated, and it is shown how using a Langevin thermostat with optimized damping values can lead to excellent agreement with reference ab initio molecular dynamics (AIMD) simulations. Structural and dynamical analyses are presented, including the studies of radial and angular distributions, homopolar bonds, and the temperature-dependent diffusivity. Herein, the usefulness of ML-driven molecular dynamics for further studies of supercooled liquid GST, with length and timescales far exceeding those that are accessible to AIMD is demonstrated.

In the information era, the demand for data storage and processing is increasing rapidly,[1] leading to active investigations of novel materials for next-generation nonvolatile memory[2–4] and neuromorphic computing chips.[5–7] Chalcogenide phase-change materials (PCMs) are leading candidates to realize these aims.[8] Recently, the first PCM-based commercial product, 3D Xpoint, has been successfully released into storage and memory markets, bridging the performance gap of flash and dynamical random access memory (DRAM). Phase-change memory utilizes a strong contrast in physical properties between the crystalline (logic "1") and amorphous states (logic "0") of PCM, such as

$Ge_2Sb_2Te_5$ (GST),[9] to store binary information. The fast and reversible switching between these two states can be realized via crystallization and amorphization processes, corresponding to writing (SET) and erasing (RESET) operations in PCM-based devices.[10] In addition, a series of continuous resistance states can be achieved via partial crystallization and amorphization, namely, cumulative SET and iterative RESET, leading to novel types of applications in neuromorphic computing in PCM-based electronics and photonics.[11–15]

The dynamical properties of PCMs are important for PCM-based devices,[16–23] since the material undergoes frequent switching during device operation. The crystallization (SET) of PCMs usually takes tens of nanoseconds (ns), whereas amorphization (RESET) is orders of magnitude faster, requiring only hundreds of picoseconds (ps).[24] A preprogramming strategy was applied in GST devices to enable an accelerated SET process.[25] Moreover, the newly designed phase-change alloy $Sc_{0.2}Sb_2Te_3$ enables a SET speed of only 0.7 ns without additional pretreatments,[26] due to the reduced stochasticity of the nucleation process via robust Sc—Te bonds.[27] With regard to the RESET process, the crystalline PCM is first melted above the melting temperatures and then the liquid PCM is quickly cooled down, reaching a supercooled liquid state. The RESET state of PCM is strongly correlated with the melting and cooling processes and is thus largely affected by the dynamical behavior of liquid and supercooled liquid states, which has prompted extensive studies on the dynamics and switching mechanisms of PCM systems.[8]

Ab initio molecular dynamics (AIMD) simulations have been applied extensively to investigate PCMs.[28] AIMD simulations have played important parts in the fundamental understanding of amorphous structures,[29–35] crystallization kinetics,[36–44] liquid-to-liquid transition,[16,17] resistance drift,[45–48] and the melting behavior.[49,50] However, the computational requirements for AIMD simulations remain an outstanding challenge. For instance, a crystallization simulation for a system of 428 atoms over 700 ps took more than half a year of real-world time using a state-of-art supercomputer.[26] This often unaffordable expense, spent in solving Schrödinger's equation for the electronic structures of PCM systems, restricts the further scaling of model system sizes, and it often precludes the study of multiple samples (for better statistics) when investigating complex physical processes. Molecular dynamics (MD) simulations with simplified, empirically fitted interatomic potential models can

Y.-X. Zhou, H.-Y. Zhang, Prof. W. Zhang
Center for Advancing Materials Performance from the Nanoscale
State Key Laboratory for Mechanical Behavior of Materials
Xi'an Jiaotong University
Xi'an 710049, China
E-mail: wzhang0@mail.xjtu.edu.cn

Y.-X. Zhou, H.-Y. Zhang, Prof. W. Zhang
Materials Studio for Neuro-Inspired Computing
School of Materials Science and Engineering
Xi'an Jiaotong University
Xi'an 710049, China

Prof. V. L. Deringer
Department of Chemistry
Inorganic Chemistry Laboratory
University of Oxford
Oxford OX1 3QR, UK
E-mail: volker.deringer@chem.ox.ac.uk

The ORCID identification number(s) for the author(s) of this article can be found under https://doi.org/10.1002/pssr.202000403.

ADVANCED
SCIENCE NEWS
www.advancedsciencenews.com

pss rrl
physica status solidi
www.pss-rapid.com

dramatically increase the speed of computations for various covalent systems. However, it is difficult to construct reliable empirical interatomic potentials for PCMs because of the large structural and chemical complexity, and it is often not feasible to accurately describe the complex interplay between different atomic environments involving three or more elements.

The development of machine-learning (ML)-based interatomic potentials has recently marked a promising advance in the studies of disordered material systems.[51] Such ML potentials reach a similar accuracy as do AIMD simulations, but at much lower computing cost (for a recent perspective on the methodology, see, for example, the study by Mueller et al.[52]). An ML potential is a mathematical representation of the potential energy surface for a given material, without a specific physically motivated functional form, instead extracting the required information from a large set of accurate reference data. The construction of a representative reference database is therefore a step of critical importance in the development of any ML potential. A variety of regression schemes and associated potential fitting frameworks have begun to be widely used, including artificial neural network (NN) models,[53,54] the Gaussian approximation potential (GAP),[55] and moment tensor potential (MTP) approaches,[56] and others.

The first NN-based potential in the PCM field was developed for the binary phase GeTe,[57] which has since shed light on the liquid dynamics,[58] crystallization kinetics,[59–61] dynamical heterogeneity,[62] aging processes,[45] nanowires,[63,64] and various physical phenomena at the amorphous–crystalline interfaces in GeTe.[65] More recently, the GAP framework together with the smooth overlap of atomic positions (SOAPs) structural descriptor[66] was used to fit an ML potential for GST.[67] Subsequently, melt-quenched GST models with up to 24 300 atoms were generated for the analysis of glassy structures with respect to quench rates and model sizes.[68] Moreover, 30 independent melt-quenched GST models were made using GAP to create sufficient statistics for the investigation of mid-gap states in amorphous GST.[69] To date, GAP-driven studies in the PCM field have mostly focused on structural characterization of liquid and quenched amorphous GST, whereas the dynamical properties of the (supercooled) liquid constitute another potentially useful topic of study.

In this article, we conducted GAP–MD simulations of liquid and supercooled liquid GST in the microcanonical (NVE) and canonical (NVT) ensembles using the large-scale atomic/molecular massively parallel simulator (LAMMPS) package.[70] The focus is strongly on NVT, for reasons specified later, using either Nosé–Hoover (NH) [71,72] or Langevin thermostats.[73] The latter was widely used in AIMD simulations of dynamical and structural properties of various PCM systems.[36,38] Using these two thermostats, we defined protocols for the simulation of (supercooled) liquid GST. In the following, we refer to these protocols as "GAP (NH)" and "GAP (L)," respectively. To implement a Langevin thermostat, a damping parameter needs to be chosen, which controls the fictitious friction in the system. The larger the damping value is, the more viscous the system will be. Seven different damping values were considered here, between 4.0×10^{-3} and $10.0 \times 10^{-3}\,\mathrm{fs}^{-1}$, corresponding to different subprotocols of GAP (L). These are referred to as GAP (LX) in the following discussions, with the running index $X = 1$ to 7, as shown in **Table 1**. For comparison, we also performed

Table 1. Thermostat setups of the GAP-based protocols as discussed in this article.

Notations of GAP-based protocols	Thermostat	Damping values [$\times 10^{-3}\,\mathrm{fs}^{-1}$]
GAP (L1)	Langevin	4.0
GAP (L2)		4.5
GAP (L3)		5.0
GAP (L4)		6.3
GAP (L5)		7.1
GAP (L6)		8.3
GAP (L7)		10
GAP (NH)	Nosé–Hoover	–

constant energy (NVE) simulations without a thermostat, which is the formally correct approach for computing dynamical properties (as discussed later).

To provide a reference for structures and dynamics of the (supercooled) liquid systems, we performed AIMD simulations using an established approach: the second-generation Car–Parrinello scheme,[74] as implemented in the Quickstep code of the CP2K package.[75] This scheme adapted a modified Langevin equation to sample the canonical distribution, where the damping parameter is split into two parts. One is an intrinsic friction coefficient to compensate the dissipative dynamics and the other is the Langevin friction coefficient,[76] both of which were well optimized referring to Born–Oppenheimer MD (BOMD) results in the previous work.[31] In the recent years, this AIMD scheme has been applied to study the crystallization dynamics of GST and yielded a growth velocity ($\approx 1\,\mathrm{m\,s}^{-1}$)[36,37] in fair agreement with the experimental work;[21] we therefore consider it to be particularly useful as a reference method against which to compare the GAP results. This is part of the reason why we strongly focus on NVT (rather than NVE) simulations in this article. In our AIMD simulations, Kohn–Sham orbitals were expanded in a Gaussian-type basis set with triple-zeta plus polarization quality, whereas plane waves with an energy cutoff of 300 Ry were used to calculate the charge density. The Perdew–Burke–Ernzerhof (PBE) functional[77] and Goedecker pseudopotentials[78] were used. Note that PBEsol[79] rather than PBE density functional theory (DFT) data served as a reference for the fitting of the GAP model that we use.[67] However, previous AIMD work using these two functionals showed rather small differences between them in how they describe structural properties of (supercooled) liquid GST.[32,67] The Brillouin zone of the supercell was sampled at the Γ point. We used identical timesteps, 2 fs, for GAP (NH), GAP (L), and AIMD simulations.

Atomic models of liquid and supercooled liquid GST were generated via melting and cooling simulations. The key results are based on a supercell which contains 198 atoms (44 Ge, 44 Sb, and 110 Te atoms) in an $18.55 \times 18.55 \times 18.55\,\text{Å}^3$ cubic box at an experimental amorphous density of $5.88\,\mathrm{g\,cm}^{-3}$. However, to evaluate possible system-size effects, we also considered three larger cubic models containing 900, 3690, and 7200 atoms (edge lengths of 30.72, 49.17, and 61.44 Å, respectively). **Figure 1**a shows a direct comparison of system sizes between the 198-atom and 7200-atom models. Starting structures of all mentioned GST

ADVANCED SCIENCE NEWS
www.advancedsciencenews.com

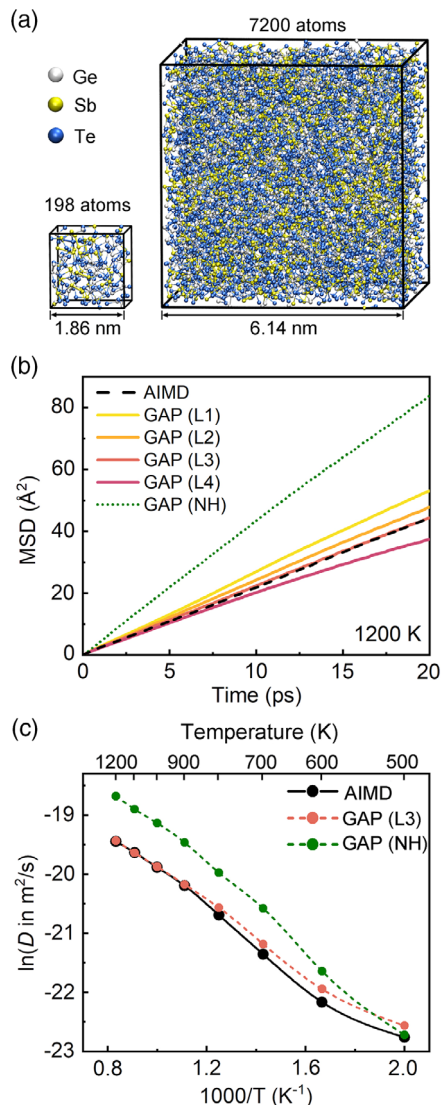**pss** rrl
physica status solidi
www.pss-rapid.com

Figure 1. a) A direct comparison of system sizes between 198-atom and 7200-atom models of GST. b) The MSD curves of GAP (NH) and different GAP (L) simulations at 1200 K were calculated to fit the MSD curve derived from AIMD simulations. Four different damping values were considered, i.e., 4.0×10^{-3}, 4.5×10^{-3}, 5.0×10^{-3}, and $6.25 \times 10^{-3}\,\mathrm{fs}^{-1}$, corresponding to four different protocols, namely, GAP (L1), GAP (L2), GAP (L3), and GAP (L4). c) The diffusion coefficients D of AIMD, GAP (L3), and GAP (NH) simulations at 1200 K as plotted in a logarithmic form over $1000/T$.

models were first randomized at 3000 K for 30 ps, and then quenched to 1200 K in 18 ps. The liquid GST models were held above the melting temperature ($\approx$900 K) and then cooled to 500 K. During cooling, the (supercooled) liquid GST systems were held at different temperatures (between 1200 and 500 K in 100 K increments). They were equilibrated for 50 ps at each increment, and then annealed for another 50 ps, where we collected data for structural and dynamical analyses. Note that the initial equilibration period is not considered in the evaluation of properties. For each of the GAP (L), GAP (NH), and AIMD protocols, four separate samples were generated with independent thermal history to improve the statistical sampling.

The mean square displacement (MSD) is usually calculated to characterize the mobility of the atoms in the simulation, defined as a function of time, t, as follows

$$\mathrm{MSD} = \langle R^2(t) \rangle = \frac{1}{N} \left\langle \sum_{i=1}^{N} |R_i(t + t_0) - R_i(t_0)|^2 \right\rangle \quad (1)$$

where R_i denotes the coordinates of atom i, t_0 is the initial point in time, N is the number of atoms, and the sum runs over all atoms. The MSD of our AIMD simulations at 1200 K was calculated based on atomic trajectories, as shown in Figure 1b. Evidently, the MSD in the GAP (NH) simulations is almost twice as large as that obtained for the AIMD ones (Figure 1b). We used varying temperature damping parameters[71] (keyword "tdamp" in LAMMPS) and Nosé chain length values ("tchain") for GAP (NH) modeling: these settings control how rapidly the temperature is relaxed and how many thermostats are in the NH thermostat chain, respectively. However, these did not affect the results strongly (Figure S1, Supporting Information). We used Langevin thermostats instead and computed the MSD using GAP (L1 to L4) protocols. It is evident that, by choosing a proper damping value, the MSD of atoms in our AIMD simulations (as a proxy for the general dynamics of the system) can be very well reproduced by GAP (L3) simulations (Figure 1b).

Furthermore, we analyzed the temperature-dependent diffusivity of GST as described by GAP (NH), GAP (L3), and AIMD protocols. The diffusion coefficient, D, is computed based on MSD results

$$D = \frac{1}{6} \frac{\partial}{\partial t} \lim_{t \to \infty} \langle R^2(t) \rangle \quad (2)$$

In addition, the diffusion coefficient also follows the Arrhenius equation, written in logarithmic form as a function of $1/T$

$$\ln D = -\frac{E}{k_B} \frac{1}{T} + \ln D_0 \quad (3)$$

where D_0 is a pre-exponential factor, k_B is the Boltzmann constant, and E denotes the activation energy. The computed logarithmic D over $1000/T$ is shown in Figure 1c. In the liquid, both GAP (L3) and AIMD predict almost the same diffusivity. A discrepancy occurs in the supercooled liquid region from 800 to 500 K, in that the atomic mobility in AIMD decreases slightly faster with T than that in the GAP (L3) simulations (Figure 1c). By contrast, a rather large deviation of diffusivity continuously exists between GAP (NH) and AIMD from 1200 to 600 K, but disappears at 500 K, which hints at a noted different description of the thermal motion in the liquid and supercooled liquid GAP (NH) simulations. We fitted our data to the Arrhenius equation and obtained the activation energy E and pre-exponential factor D_0 for AIMD, GAP (L3), and GAP (NH), respectively, as shown in **Table 2**. The activation energies calculated from AIMD and GAP (L) protocols are in fair agreement with that derived from experiments ($E = 0.266$ eV).[80]

We note that computed diffusion coefficients of GST may strongly depend on the simulation protocol, as shown in Figure S2, Supporting Information—which includes our AIMD data and others[80,81] with different functionals and thermostats, as well as experimental data for GST alloys, measured using an oscillating cup viscometer.[80] The absolute diffusivities from

ADVANCED SCIENCE NEWS
www.advancedsciencenews.com

pssrrl
physica status solidi
www.pss-rapid.com

Table 2. The calculated activation energy and pre-exponential factor for three different protocols.

Protocol	E [eV]	D_0 [$\times 10^{-10}$ m^2 s^{-1}]
AIMD	0.260	446
GAP (L3)	0.241	373
GAP (NH)	0.305	1674

GAP (NH) are further from the experimental values, whereas the slopes of both GAP (NH) and experimental results with temperature are almost the same. In addition, we performed simulations in which we switched off the thermostat after equilibration at the target temperatures, followed by GAP–MD simulations in the NVE ensemble, leading to very similar results as our GAP (NH) simulations and the AIMD (NVE) simulations reported in the study by Rizzi et al.[81] Therefore, on the one hand, the temperature dependence of diffusivity is well recovered by AIMD (NVE), GAP (NH), and GAP (NVE); on the other hand, by carefully calibrating the settings of the Langevin thermostat, GAP (L) simulations show the closest absolute agreement of diffusivity with experimental results at 900 and 1000 K.

We also note that studies of crystallization kinetics of PCMs require the use of well-optimized thermostats.[36–38,42–44] As mentioned earlier, AIMD simulations using a second-generation Car–Parrinello scheme and an Langevin thermostat[74] show an average growth rate of ≈ 1 m s^{-1} at ≈ 600 K, which increases to ≈ 1.5 m s^{-1} at ≈ 700 K,[36,37] in good agreement with ultrafast differential scanning calorimetry (DSC) measurements.[21] Therefore, large-scale GAP (L) simulations that closely mirror the AIMD reference are expected to lead to accurate descriptions of switching behavior of supercooled liquid GST.

To analyze the atomistic structures obtained from the different simulations, we studied short- and medium-range structural features based on the radial distribution function (RDF; **Figure 2**a) and normalized angle distribution function (ADF;

Figure 2b). There is an excellent agreement of RDF and ADF between the two GAP protocols, indicating the near-independence of local structural properties of liquid and supercooled liquid GST from the choice of thermostats. The overall distribution of RDF and ADF from both GAP protocols is consistent with AIMD, albeit small deviations remain. In AIMD, there are lower coordination numbers within the first atomic shell compared to GAP, measured by integration of the RDF up to the first minimum, and this effect becomes more pronounced at lower temperatures, such as 600 K (Figure 2a). In all three systems, atoms are mostly in defective-octahedral environments, correlated with a broad peak at 90° in the ADF (Figure 2b). However, a slight preference for tetrahedral motifs appears in AIMD at 600 K in comparison to GAP–MD, as the AIMD ADF shifts slightly to larger bond angles and has a broader shoulder at $\approx 109°$. System size effects were also evaluated based on the same dynamical and structural analyses at 1200 K. We observed very similar MSD, RDF, and ADF in all four models with varying system sizes, i.e., 198, 900, 3690, or 7200 atoms, when carrying out GAP (L3) simulations. Therefore, our discussions, based on 198-atom models, are unlikely to be affected by system size effects.

The analysis of homopolar bonds (Ge—Ge, Sb—Sb, and Te—Te) reveals subtle structural differences between the GAP and AIMD simulations, as shown in Figure 2c. The statistics of homopolar bonds, intrinsically correlated with the distributions of primitive rings and local structural motifs,[27] are a good indicator to describe short-range ordering, chemical-bonding features, and dynamical properties of the system. The choice of cutoffs used in the bond analysis for (supercooled) liquid GST is in line with the study by Caravati et al.[31] In the liquid state above 900 K, the fractions of homopolar bonds in all the three simulation protocols are nearly the same and decrease steadily as the temperature goes down. When it comes to the supercooled liquid regime, the fraction of homopolar bonds in AIMD continues to slowly decrease with temperature, and then remains at $\approx 11\%$
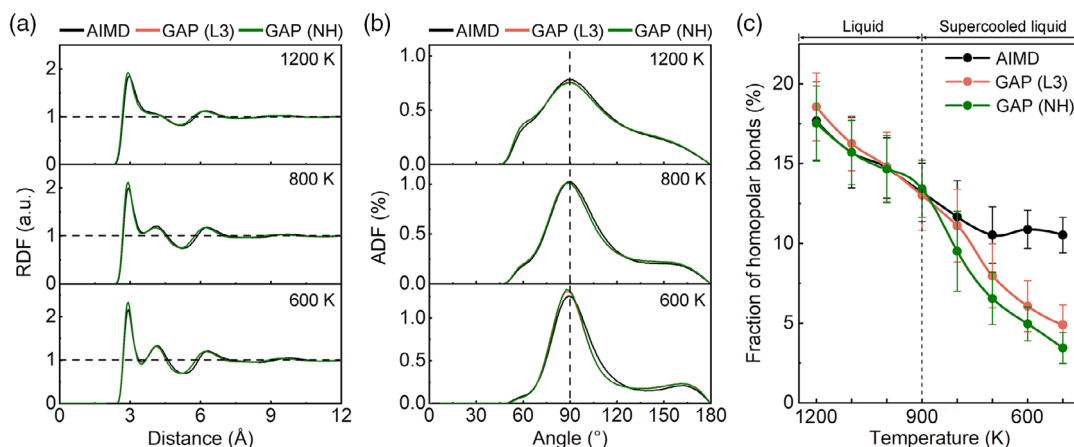

Figure 2. Structural characterization of liquid and supercooled liquid GST as described using different modeling methods, including GAP (NH), GAP (L3), and the AIMD reference. a) RDF and b) normalized ADF for different protocols at 1200, 800, and 600 K, respectively. c) The fractions of homopolar bonds in three different (supercooled) liquid GST structures (generated via AIMD, GAP (L3), and GAP (NH) simulations). Each data point indicates an averaged value over four independent samples at a given temperature. The error bars, expressed as standard deviations of the calculated fraction, represent the variations over 20 000 snapshots taken from four separate samples (5000 snapshots from each sample). Lines between data points are guides to the eye.

**ADVANCED
SCIENCE NEWS**
www.advancedsciencenews.com

pss rrl
physica status solidi
www.pss-rapid.com

below 700 K. However, an abrupt decrease in homopolar bonds is observed in GAP (NH) at 800 K, and the fast decrease in the number of homopolar bonds continues upon further cooling, leading to gradually enlarged deviations from AIMD. A similar drop and a swift decrease also appear in GAP (L) but start at 700 K, which results in relatively more homopolar bonds found in GAP (L) than in GAP (NH). The fractions of homopolar bonds in GAP (L) and GAP (NH) are ≈5% and ≈3%, respectively, at 500 K, much smaller than the AIMD result (≈11%). Furthermore, the statistics of different types of bonds reveal that Sb—Sb bonds and Te—Te bonds contributed most to this discrepancy in both GAP (L) and GAP (NH) protocols at lower temperatures (500 and 600 K) (Figure S3, Supporting Information). In summary, the GAP (L3) protocols are structurally feasible in liquid state (above 900 K) and supercooled liquid state at high temperature (700–900 K). As the temperature decreases to 700 K and below, both structural and dynamical deviations appear in GAP (L3) protocols in comparison to AIMD.

We now study the supercooled liquid in more detail. To calibrate the damping value for the accurate description of the supercooled dynamics as compared to AIMD, we used the same strategy as shown in Figure 1b. We chose different damping values and calculated the MSD results of different supercooled liquid GAP (L) protocols at 600 K (**Figure 3**a). The MSD curve of GAP (L6) overlaps with the AIMD reference, hinting at similar

supercooled liquid dynamics in both simulations. We further compared the short- and medium-range structural features of AIMD, GAP (L3), and GAP (L6) protocols via RDF and ADF analyses (Figure 3b,c). Both GAP (L3) and GAP (L6) led to almost the same RDF and ADF, whereas a visible deviation still exists compared to AIMD. The fraction of homopolar bonds increased in GAP (L6) compared to that in GAP (L3), but was still lower than that in AIMD. In short, by increasing the damping value for the Langevin thermostat, we can access dynamical properties of supercooled liquid GST at 600 K in excellent agreement with AIMD. In contrast, structural deviations at low temperatures between GAP–MD and AIMD can be mitigated but cannot be eliminated fully.

Following the strategy discussed in the context of Figure 1a and 3a, we also optimized the damping values at other temperatures during melting and cooling, and thus propose an approach to simulate liquid and supercooled liquid GST using adaptive GAP (L) protocols that aim to match the AIMD result most closely. We used three different thermostat settings during the simulation, i.e., GAP (L3) for the liquid from 1200 to 900 K, GAP (L4) for the high temperature supercooled liquid from 800 to 700 K, and GAP (L6) for the low temperature supercooled liquid from 600 to 500 K (**Figure 4**a). Calculated diffusion coefficients are shown in Figure 4b. It is evident that, using these calibrated damping values, we can access the dynamics of liquid
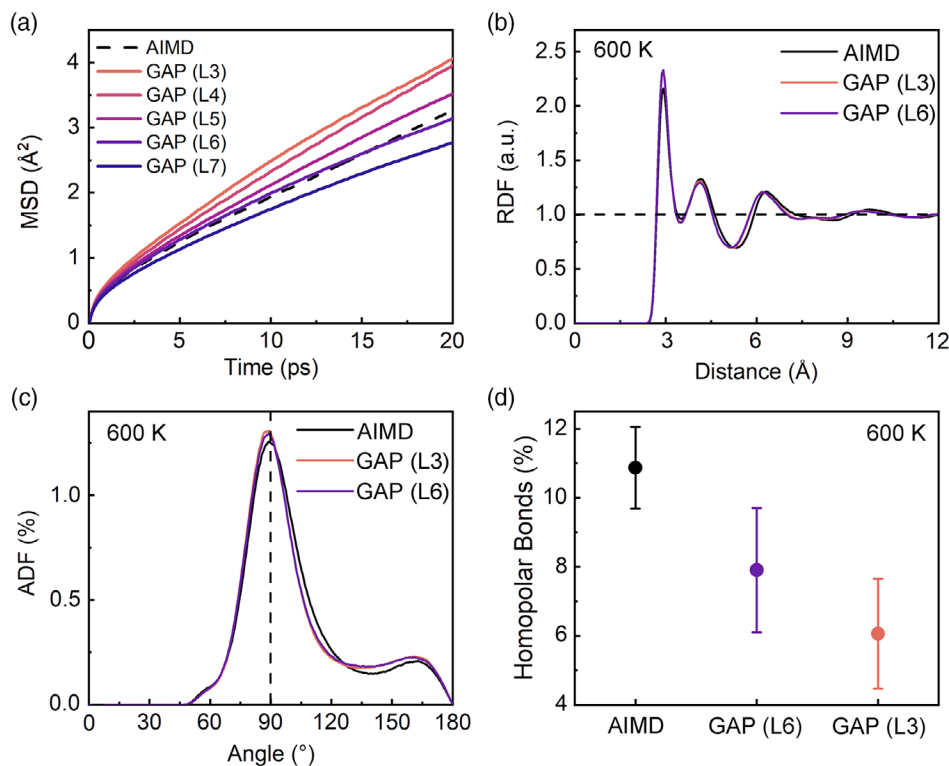

Figure 3. Structure and dynamics of supercooled liquid GST at 600 K. a) A series of MSD curves were calculated, derived from different GAP (L) protocols, including GAP (L3), GAP (L4), GAP (L5), GAP (L6), and GAP (L7). The MSD curve of the GAP (L6) simulation overlaps best with that of the AIMD one at 600 K. b) RDF analysis and c) ADF analysis are performed for AIMD, GAP (L3), and GAP (L6) structures. d) The statistics of homopolar bonds are analyzed for three protocols. The error bars indicate the variations over 20 000 snapshots taken from four independent samples (5000 snapshots from each sample) at 600 K.
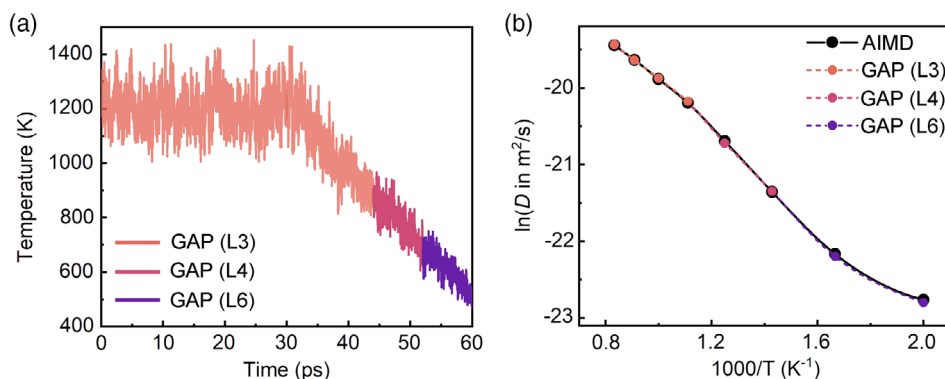
Figure 4. The strategy of using GAP (L) protocols of different damping values to simulate different (supercooled) liquid GST. a) The temperature profile of melting and quenching processes in the GAP (L) protocols utilized to generate liquid and supercooled liquid GST models. Three different subprotocols were used in three different temperature regimes during the melting and quenching processes: GAP (L3) (from 1200 to 900 K), GAP (L4) (from 900 to 700 K), and GAP (L6) (from 700 to 500 K). b) The calculated diffusion coefficient D of GAP (L) protocols, plotted in logarithmic form as a function of $1000/T$, during quenching from 1200 to 500 K, is consistent with those derived from the reference AIMD. Lines between data points are guides to the eye.

and supercooled liquid GST in very good agreement with AIMD throughout the relevant range of temperatures. Yet, a structural discrepancy between GAP (L) and AIMD remains below 700 K, which requires further investigation.

In conclusion, we have shown that the combination of the GAP ML potential and Langevin MD with a properly chosen damping value can describe supercooled liquid GST in good agreement with AIMD simulations, the latter being the current de facto standard in atomistic modeling of PCMs. We note that in principle, any type of reference, either from high-level simulations or from experiment, can serve as a reference to optimize the thermostat setups in GAP-based modeling. Our results and analyses hint toward the usefulness of ML-driven simulations for further studies of (supercooled) liquid GST, as well as more complex physicochemical phenomena during switching in memory devices.

Supporting Information

Supporting Information is available from the Wiley Online Library or from the author.

Acknowledgements

Conflict of Interest

The authors declare no conflict of interest.

Keywords

[1] H. S. Wong, S. Salahuddin, *Nat. Nanotechnol.* **2015**, *10*, 191.

[2] M. Wuttig, N. Yamada, *Nat. Mater.* **2007**, *6*, 824.

[3] M. H. Lankhorst, B. W. Ketelaars, R. A. Wolters, *Nat. Mater.* **2005**, *4*, 347.

[4] C. Ríos, M. Stegmaier, P. Hosseini, D. Wang, T. Scherer, C. D. Wright, H. Bhaskaran, W. H. P. Pernice, *Nat. Photonics* **2015**, *9*, 725.

[5] K. Ding, J. Wang, Y. Zhou, H. Tian, L. Lu, R. Mazzarello, C. Jia, W. Zhang, F. Rao, E. Ma, *Science* **2019**, *366*, 210.

[6] A. Sebastian, M. Le Gallo, R. Khaddam-Aljameh, E. Eleftheriou, *Nat. Nanotechnol.* **2020**, *15*, 529.

[7] S. Ambrogio, P. Narayanan, H. Tsai, R. M. Shelby, I. Boybat, C. di Nolfo, S. Sidler, M. Giordano, M. Bodini, N. C. P. Farinha, B. Killeen, C. Cheng, Y. Jaoudi, G. W. Burr, *Nature* **2018**, *558*, 60.

[8] W. Zhang, R. Mazzarello, M. Wuttig, E. Ma, *Nat. Rev. Mater.* **2019**, *4*, 150.

[9] N. Yamada, E. Ohno, N. Nishiuchi, N. Akahira, M. Takao, *J. Appl. Phys.* **1991**, *69*, 2849.

[10] P. Zalden, A. von Hoegen, P. Landreman, M. Wuttig, A. M. Lindenberg, *Chem. Mater.* **2015**, *27*, 5641.

[11] W. Zhang, R. Mazzarello, E. Ma, *MRS Bull.* **2019**, *44*, 686.

[12] W. Zhang, M. Wuttig, *Phys. Status Solidi RRL* **2019**, *13*, 1900130.

[13] M. Wuttig, H. Bhaskaran, T. Taubner, *Nat. Photonics* **2017**, *11*, 465.

[14] Z. Wang, H. Wu, G. W. Burr, C. S. Hwang, K. L. Wang, Q. Xia, J. J. Yang, *Nat. Rev. Mater.* **2020**, *5*, 173.

[15] Q. Xia, J. J. Yang, *Nat. Mater.* **2019**, *18*, 309.

[16] P. Zalden, F. Quirin, M. Schumacher, J. Siegel, S. Wei, A. Koc, M. Nicoul, M. Trigo, P. Andreasson, H. Enquist, M. J. Shu, T. Pardini, M. Chollet, D. Zhu, H. Lemke, I. Ronneberger, J. Larsson, A. M. Lindenberg, H. E. Fischer, S. Hau-Riege, D. A. Reis, R. Mazzarello, M. Wuttig, K. Sokolowski-Tinten, *Science* **2019**, *364*, 1062.

[17] F. Rao, W. Zhang, E. Ma, *Science* **2019**, *364*, 1032.

[18] J. Pries, S. Wei, M. Wuttig, P. Lucas, *Adv. Mater.* **2019**, *31*, 1900784.

[19] J. Pries, O. Cojocaru-Mirédin, M. Wuttig, *MRS Bull.* **2019**, *44*, 699.

[20] J. Orava, D. W. Hewak, A. L. Greer, *Adv. Funct. Mater.* **2015**, *25*, 4851.

[21] J. Orava, A. L. Greer, B. Gholipour, D. W. Hewak, C. E. Smith, *Nat. Mater.* **2012**, *11*, 279.

[22] A. Sebastian, M. Le Gallo, D. Krebs, *Nat. Commun.* **2014**, *5*, 4314.

[23] M. Salinga, E. Carria, A. Kaldenbach, M. Bornhöfft, J. Benke, J. Mayer, M. Wuttig, *Nat. Commun.* **2013**, *4*, 2371.

[24] H. S. P. Wong, S. Raoux, S. Kim, J. Liang, J. P. Reifenberg, B. Rajendran, M. Asheghi, K. E. Goodson, *Proc. IEEE* **2010**, *98*, 2201.

[25] D. Loke, T. H. Lee, W. J. Wang, L. P. Shi, R. Zhao, Y. C. Yeo, T. C. Chong, S. R. Elliott, *Science* **2012**, *336*, 1566.

[26] F. Rao, K. Ding, Y. Zhou, Y. Zheng, M. Xia, S. Lv, Z. Song, S. Feng, I. Ronneberger, R. Mazzarello, W. Zhang, E. Ma, *Science* **2017**, *358*, 1423.

[27] G. M. Zewdie, Y. Zhou, L. Sun, F. Rao, V. L. Deringer, R. Mazzarello, W. Zhang, *Chem. Mater.* **2019**, *31*, 4008.

[28] W. Zhang, V. L. Deringer, R. Dronskowski, R. Mazzarello, E. Ma, M. Wuttig, *MRS Bull.* **2015**, *40*, 856.

[29] Y. Zhou, L. Sun, G. M. Zewdie, R. Mazzarello, V. L. Deringer, E. Ma, W. Zhang, *J. Mater. Chem. C* **2020**, *8*, 3646.

[30] S. Hu, J. Xiao, J. Zhou, S. R. Elliott, Z. Sun, *J. Mater. Chem. C* **2020**, *8*, 6672.

[31] S. Caravati, M. Bernasconi, T. D. Kühne, M. Krack, M. Parrinello, *Appl. Phys. Lett.* **2007**, *91*, 171906.

[32] J. Akola, R. Jones, *Phys. Rev. B* **2007**, *76*, 235201.

[33] M. Xu, Y. Cheng, H. Sheng, E. Ma, *Phys. Rev. Lett.* **2009**, *103*, 195502.

[34] W. Zhang, I. Ronneberger, Y. Li, R. Mazzarello, *Monatsh. Chem.* **2013**, *145*, 97.

[35] W. Zhang, E. Ma, *Nat. Mater.* **2018**, *17*, 654.

[36] I. Ronneberger, W. Zhang, H. Eshet, R. Mazzarello, *Adv. Funct. Mater.* **2015**, *25*, 6407.

[37] I. Ronneberger, W. Zhang, R. Mazzarello, *MRS Commun.* **2018**, *8*, 1018.

[38] W. Zhang, I. Ronneberger, P. Zalden, M. Xu, M. Salinga, M. Wuttig, R. Mazzarello, *Sci. Rep.* **2014**, *4*, 6529.

[39] I. Ronneberger, Y. Chen, W. Zhang, R. Mazzarello, *Phys. Status Solidi RRL* **2018**, *13*, 1800552.

[40] T. H. Lee, S. R. Elliott, *Phys. Rev. Lett.* **2011**, *107*, 145702.

[41] J. Hegedüs, S. R. Elliott, *Nat. Mater.* **2008**, *7*, 399.

[42] J. Kalikka, J. Akola, R. O. Jones, *Phys. Rev. B* **2016**, *94*, 134105.

[43] J. Kalikka, J. Akola, R. O. Jones, *Phys. Rev. B* **2014**, *90*, 184109.

[44] J. Kalikka, J. Akola, J. Larrucea, R. O. Jones, *Phys. Rev. B* **2012**, *86*, 144113.

[45] S. Gabardi, S. Caravati, G. C. Sosso, J. Behler, M. Bernasconi, *Phys. Rev. B* **2015**, *92*, 054201.

[46] Y. Chen, L. Sun, Y. Zhou, G. M. Zewdie, V. L. Deringer, R. Mazzarello, W. Zhang, *J. Mater. Chem. C* **2020**, *8*, 71.

[47] J. Y. Raty, W. Zhang, J. Luckas, C. Chen, R. Mazzarello, C. Bichara, M. Wuttig, *Nat. Commun.* **2015**, *6*, 7467.

[48] W. Zhang, E. Ma, *Mater. Today* https://doi.org/10.1016/j.mattod. 2020.07.016.

[49] X.-P. Wang, X.-B. Li, N.-K. Chen, J. Bang, R. Nelson, C. Ertural, R. Dronskowski, H.-B. Sun, S. Zhang, *npj Comput. Mater.* **2020**, *6*, 31.

[50] X.-B. Li, X. Q. Liu, X. Liu, D. Han, Z. Zhang, X. D. Han, H.-B. Sun, S. B. Zhang, *Phys. Rev. Lett.* **2011**, *107*, 015501.

[51] V. L. Deringer, M. A. Caro, G. Csányi, *Adv. Mater.* **2019**, *31*, 1902765.

[52] T. Mueller, A. Hernandez, C. Wang, *J. Chem. Phys.* **2020**, *152*, 050902.

[53] J. Behler, M. Parrinello, *Phys. Rev. Lett.* **2007**, *98*, 146401.

[54] L. Zhang, J. Han, H. Wang, R. Car, E. Weinan, *Phys. Rev. Lett.* **2018**, *120*, 143001.

[55] A. P. Bartók, M. C. Payne, R. Kondor, G. Csányi, *Phys. Rev. Lett.* **2010**, *104*, 136403.

[56] A. V. Shapeev, *Multiscale Model. Simul.* **2016**, *14*, 1153.

[57] G. C. Sosso, G. Miceli, S. Caravati, J. Behler, M. Bernasconi, *Phys. Rev. B* **2012**, *85*, 174103.

[58] G. C. Sosso, J. Behler, M. Bernasconi, *Phys. Status Solidi B* **2012**, *249*, 1880.

[59] G. C. Sosso, M. Salvalaglio, J. Behler, M. Bernasconi, M. Parrinello, *J. Phys. Chem. C* **2015**, *119*, 6428.

[60] G. Sosso, G. Miceli, S. Caravati, F. Giberti, J. Behler, M. Bernasconi, *J. Phys. Chem. Lett.* **2013**, *4*, 4241.

[61] S. Gabardi, G. G. Sosso, J. Behler, M. Bernasconi, *Faraday Discuss.* **2019**, *213*, 287.

[62] G. C. Sosso, J. Colombo, J. Behler, E. Del Gado, M. Bernasconi, *J. Phys. Chem. B* **2014**, *118*, 13621.

[63] S. Gabardi, E. Baldi, E. Bosoni, D. Campi, S. Caravati, G. C. Sosso, J. Behler, M. Bernasconi, *J. Phys. Chem. C* **2017**, *121*, 23827.

[64] E. Bosoni, D. Campi, D. Donadio, G. C. Sosso, J. Behler, M. Bernasconi, *J. Phys. D: Appl. Phys.* **2020**, *53*, 054001.

[65] G. C. Sosso, M. Bernasconi, *MRS Bull.* **2019**, *44*, 705.

[66] A. P. Bartók, R. Kondor, G. Csányi, *Phys. Rev. B* **2013**, *87*, 184115.

[67] F. C. Mocanu, K. Konstantinou, T. H. Lee, N. Bernstein, V. L. Deringer, G. Csányi, S. R. Elliott, *J. Phys. Chem. B* **2018**, *122*, 8998.

[68] F. C. Mocanu, K. Konstantinou, S. R. Elliott, *J. Phys. D: Appl. Phys.* **2020**, *53*, 244002.

[69] K. Konstantinou, F. C. Mocanu, T.-H. Lee, S. R. Elliott, *Nat. Commun.* **2019**, *10*, 3065.

[70] S. Plimpton, *J. Comput. Phys.* **1995**, *117*, 1.

[71] S. Nosé, *Mol. Phys.* **1984**, *52*, 255.

[72] W. G. Hoover, *Phys. Rev. A* **1985**, *31*, 1695.

[73] T. Schneider, E. Stoll, *Phys. Rev. B* **1978**, *17*, 1302.

[74] T. D. Kühne, M. Krack, F. R. Mohamed, M. Parrinello, *Phys. Rev. Lett.* **2007**, *98*, 066401.

[75] J. Hutter, M. Iannuzzi, F. Schiffmann, J. VandeVondele, *Rev. Comput. Mol. Sci.* **2014**, *4*, 15.

[76] T. Musso, S. Caravati, J. Hutter, M. Iannuzzi, *Eur. Phys. J. B* **2018**, *91*, 148.

[77] J. P. Perdew, K. Burke, M. Ernzerhof, *Phys. Rev. Lett.* **1996**, *77*, 3865.

[78] S. Goedecker, M. Teter, J. Hutter, *Phys. Rev. B* **1996**, *54*, 1703.

[79] J. Perdew, A. Ruzsinszky, G. Csonka, O. Vydrov, G. Scuseria, L. Constantin, X. Zhou, K. Burke, *Phys. Rev. Lett.* **2008**, *100*, 136406.

[80] M. Schumacher, H. Weber, P. Jóvári, Y. Tsuchiya, T. G. A. Youngs, I. Kaban, R. Mazzarello, *Sci. Rep.* **2016**, *6*, 27434.

[81] M. Rizzi, N. Ciocchini, S. Caravati, M. Bernasconi, P. Fantini, D. Ielmini, *IEDM Tech. Dig.* **2015**, 21.